

pubs.acs.org/journal/apchd5 Article

Silicon Nitride Waveguides with Intrinsic Single-Photon Emitters for Integrated Quantum Photonics

Alexander Senichev,* Samuel Peana, Zachariah O. Martin, Omer Yesilyurt, Demid Sychev, Alexei S. Lagutchev, Alexandra Boltasseva, and Vladimir M. Shalaev*



Cite This: https://doi.org/10.1021/acsphotonics.2c00750



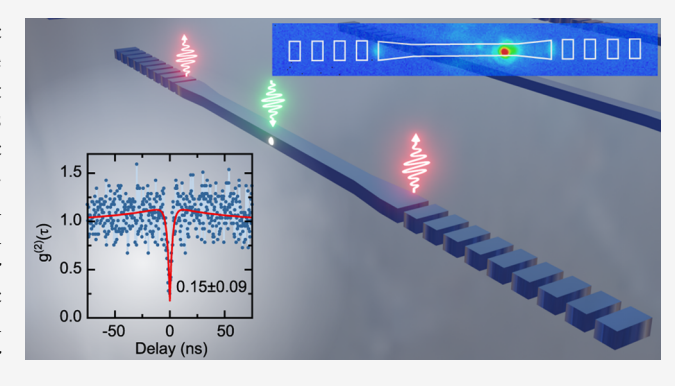
ACCESS I

Metrics & More

Article Recommendations

SI Supporting Information

ABSTRACT: The recent discovery of room-temperature intrinsic single-photon emitters in silicon nitride $(SiN)^1$ provides a unique opportunity for seamless monolithic integration of quantum light sources with the well-established SiN photonic platform. In this work, we successfully demonstrate the integration of intrinsic quantum emitters with planar waveguides composed of low-autofluorescence SiN and demonstrate single-photon emission coupling into the waveguide mode. The coupling of single-photon emission to the waveguide mode is confirmed by second-order autocorrelation measurements of light outcoupled off the photonic chip by grating couplers. Fitting the second-order autocorrelation histogram yields $g^{(2)}(0) = 0.15 \pm 0.09$ without spectral filtering or background correction, the outcoupled photon rate derived from



saturation measurements is found to be 6×10^3 counts per second. This demonstrates the first successful coupling of photons from monolithically integrated SiN intrinsic single-photon emitters with waveguides composed of the same material. The results of our work pave the way toward the realization of scalable, technology-ready quantum photonic integrated circuitry efficiently interfaced with solid-state quantum emitters.

KEYWORDS: solid-state quantum emitters, single-photon emitters, silicon nitride, waveguides, quantum photonic integrated circuits

INTRODUCTION

Photonic quantum systems employ photons to encode and transmit quantum information and distribute quantum entanglement through interactions with other photons and various stationary qubits. Solid-state quantum emitters are fundamental resources for photon-based quantum information technologies. They can serve as on-demand single-photon sources, components of atomic memories, quantum repeaters, and quantum sensors. 1-6 Realization of these devices requires photonic elements, which would enable efficient interfacing between light and matter, high collection efficiency, low-loss routing of photons, and interconnection between photonic qubits for quantum logic operations.^{7,8} Direct coupling of quantum emitters to quantum photonic integrated circuits (QPICs) offers scalability and stability to photonic elements. This in turn may enable a high density of on-chip photonic qubit sources and the level of performance required for practical applications in the quantum domain.⁸⁻¹⁰

The possibility to integrate quantum emitters with QPICs depends critically on the properties of the host materials. Wellestablished solid-state quantum emitters include III–V semiconductor quantum dots (QDs)^{7,11,12} and defect-based color centers in diamond,^{13–15} silicon carbide (SiC),^{16–19} and hexagonal boron nitride (hBN),^{20–22} to name a few. The

high brightness, single-photon purity, indistinguishability, and optically addressable spins of these quantum emitters make them promising for applications in quantum communication, computing, and sensing. Some of these materials, which host quantum emitters, can also be used for the fabrication of photonic components for QPICs. For example, diamond QPICs with embedded color centers were recently used to demonstrate on-chip cavity-enhanced single-photon sources and quantum memories. 5,23-25 III-V semiconductors, SiC and hBN, have also been extensively studied as platforms with intrinsic quantum emitters, which are also capable of supporting QPIC elements such as waveguides, directional couplers, and resonant cavities. However, these materials can only support the fabrication of a limited variety of photonic components, making them insufficient for full-fledged QPICs. Hence, on-chip integration of common solid-state quantum emitters typically relies on hybrid approaches

Received: May 17, 2022



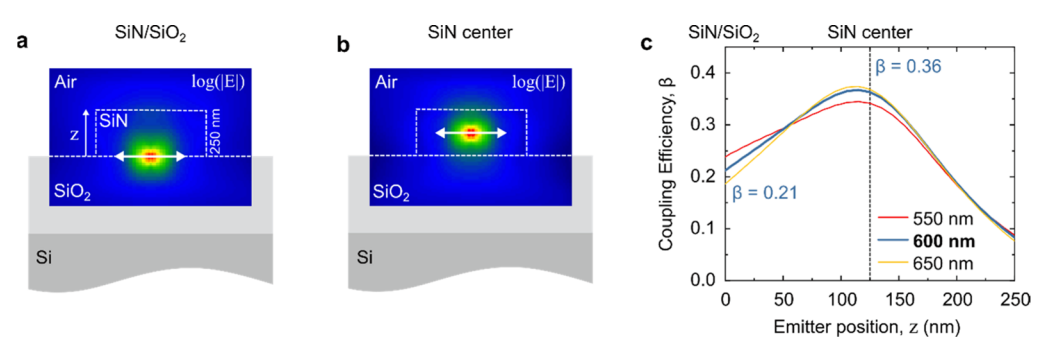


Figure 1. Coupling efficiency simulation of an intrinsic quantum emitter in a SiN waveguide. (a) Interface-positioned dipole with the simulated normalized electric field. (b) Center-positioned dipole and its normalized electric field. For both positions, the emitter dipole is oriented in the plane of the substrate and orthogonal to the waveguide axis and is indicated with the white two-headed arrows. (c) Simulated coupling efficiency as a function of the dipole vertical position z within the waveguide for three wavelengths 550, 600, and 650 nm.

combining materials that host quantum emitters and material platforms that are well-developed for QPICs.^{29,30}

Currently, the most developed, technology-driven material platforms for integrated photonics include silicon on insulator (SOI), silicon nitride (SiN), lithium niobate (LiNbO₃), and aluminum nitride (AlN).8 Large-scale hybrid integration was recently demonstrated for quantum emitters in diamond coupled to AlN photonic circuitry.31 Semiconductor QDs were also integrated with LiNbO₃ photonic devices.³² Hybrid integration with SiN photonic circuitry has been demonstrated for various quantum emitters such as semiconductor QDs, 33-36 color centers in 2D materials, 37-39 and nanodiamonds. 40,41 Although the hybrid integration approach provides more flexibility in the realization of large-scale QPICs and has shown tremendous progress, it also faces inevitable challenges related to photon losses due to the interfacing of dissimilar materials and the complex integration geometries and fabrication procedures required.

Consequently, particular attention has been paid to engineering intrinsic or directly embedded quantum emitters in material platforms, which are suitable for the realization of QPICs. Such intrinsic quantum emitters have been discovered in gallium nitride, 42,43 aluminum nitride, 44–47 and silicon. Monolithic integration of these intrinsic emitters with QPICs offers high coupling efficiencies along with simplified fabrication processes, and it promises to enable the long-awaited industrial-scale quantum photonic circuitry.

Our group has recently discovered bright, stable, linearly polarized, and high-purity sources of single-photon emission at room temperature in nitrogen-rich SiN. Stochiometric silicon nitride (Si₃N₄) is a leading integrated photonics material platform that is technologically mature and CMOS compatible and offers low propagation and insertion losses. It is wellestablished for linear and nonlinear integrated optics^{51–53} and has recently emerged as a potential platform for integrated quantum photonics. 8,54,55 Importantly, Si_3N_4 photonic components exhibit ultra-low losses, which is especially critical for the realization of large-scale QPICs. Recent examples of experimentally realized Si₃N₄-based QPIC elements include on-chip frequency converters, phase shifters, and beam splitters, all combined in a fully reconfigurable quantum photonic processor.⁵⁴ Consequently, Si₃N₄ is the material of choice for the development of the next generation of photonic quantum computers based on ultra-low loss waveguides by photonic quantum technology companies such as Xanadu⁸⁰ and QuiX.5

Here, we report on the development of low-autofluorescence SiN planar waveguides containing intrinsic single-photon sources that were recently discovered in our previous work. While stoichiometric Si₃N₄ provides ultra-low loss photonic waveguides, the non-stoichiometric nitrogen-rich SiN used in our work offers substantially lower background fluorescence in the visible spectral range. This facilitates the integration with visible-wavelength quantum emitters. 1,58 In this work, we demonstrate individually addressable intrinsic single-photon sources in SiN photonic structures. To accomplish this, we grew low-autofluorescence SiN films with bright, stable, roomtemperature quantum emitters on SiO2-coated silicon substrates. From this film, we fabricated SiN waveguides with onchip grating couplers. The photophysical properties of SiN single-photon emitters in the waveguides were characterized by collecting photons both directly outcoupled to the far field or coupled to the waveguide mode and then outcoupled off-chip by grating couplers. Our findings show that quantum emitters retain their photophysical properties after the waveguide fabrication procedure. With these results, we demonstrate the first successful realization of low-autofluorescing SiN waveguides with intrinsic quantum emitters and the coupling of single-photon emission to a waveguide mode.

■ RESULTS AND DISCUSSION

Utilizing the previously developed single photon emitter creation approach, we grow a material stack with lowautofluorescence SiN containing intrinsic quantum emitters. This involves the growth of nitrogen-rich SiN films using highdensity plasma chemical vapor deposition on commercially available silicon dioxide (SiO₂)-coated silicon substrates. Subsequently, the intrinsic single photon emitters in SiN are generated by post-growth rapid thermal annealing (RTA) for 120 s at a temperature of 1100 °C in a nitrogen atmosphere. Ellipsometry characterization of the samples revealed that the refractive index n of the resultant SiN films was ~ 1.7 . This value is lower than the typical refractive index of n = 2.0reported for stoichiometric Si₃N₄ due to the need for lowautofluorescence SiN. 58,59 The waveguides were designed and simulated using a commercial Maxwell solver. We simulated the coupling efficiency β given by the ratio of the light intensity coupled to the fundamental mode of the waveguide to the total emitted light intensity from the dipole. The simulation was performed for various positions and orientations of the dipole within the waveguide (Supporting Information, Figure S2). From a previous work, we expect the quantum emitters to be

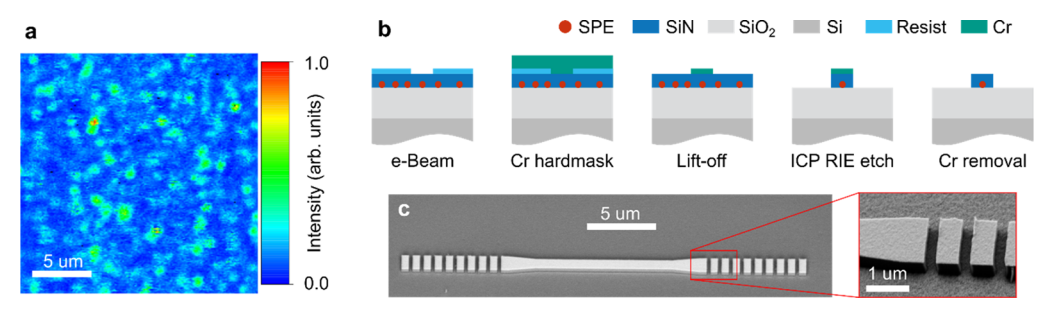


Figure 2. Fabrication of low-autofluorescence SiN waveguides with intrinsic quantum emitters. (a) $20 \times 20 \ \mu\text{m}^2$ confocal PL intensity map of the SiN sample before waveguide fabrication, revealing a high density of isolated emitters. (b) Fabrication process used to create waveguides out of continuous SiN films containing intrinsic quantum emitters. (c) SEM images of a fabricated waveguide with an enlarged view of a grating coupler segment.

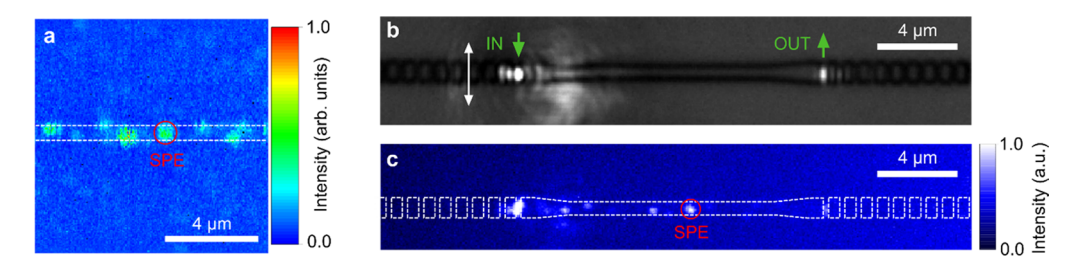


Figure 3. Spatial distribution of waveguide-integrated quantum emitters. (a) $10 \times 10 \ \mu m^2$ confocal PL intensity map of the SiN sample after the fabrication of a waveguide. The white dotted lines show the outline of the waveguide. (b) CCD image showing the laser light coupled into the waveguide through a grating coupler and outcoupled from the other end. (c) CCD image of the same waveguide as in (b) with the excitation light suppressed using a 550 nm long pass filter. Fluorescence from individual single-photon emitters is clearly visible. The red circle indicates the quantum emitter selected for further analysis.

located at the interface between the SiO₂ and SiN layers and the dipole oriented in the plane of the substrate. Simulation results for an interface-positioned quantum emitter (Figure 1a) show a coupling efficiency of β = 21% of the emission from the dipole source to the fundamental waveguide mode for the given SiN refractive index of 1.7 and the central wavelength of 600 nm (Figure 1c). It is important to note that this value for coupling efficiency β for the given material system is already better than those typically reported for hybrid integration geometries.^{39,60} For hybrid approaches, the simulated coupling efficiencies for an emitter placed on the top of a SiN waveguide⁶⁰ and embedded into a SiN waveguide³⁹ were found to be a few percent and up to approximately 19%, respectively. A near-optimal coupling efficiency to the fundamental waveguide mode for the given waveguide geometry can be obtained by placing a dipole at the center of the waveguide, yielding β = 36% (Figure 1b,c). Moreover, the coupling efficiency of intrinsic SiN quantum emitters can be even further improved by precision positioning of an emitter into topology-optimized couplers, as has been shown theoretically.⁶¹ This is the subject of ongoing efforts and is outside the scope of this work. We also simulated the outcoupling efficiency from the grating couplers at 600 nm, resulting in $\eta = 22\%$.

The photophysical properties of quantum emitters in SiN samples were characterized before waveguide fabrication using our custom-made scanning confocal microscope equipped with a Hanbury–Brown–Twiss (HBT) setup (see the Methods section for details). The observed emitters exhibit properties in line with those previously reported. The confocal photoluminescence (PL) map shown in Figure 2a reveals bright isolated emitters with an average density of approximately 10 emitters per 100 μ m². The dimensions of the simulated

waveguides and the high density of emitters ensures a high probability that each waveguide contains several emitters without any spatial alignment procedure. A large array of waveguides was fabricated using conventional electron beam lithography and inductively coupled plasma reactive ion etching (ICP RIE). The fabrication approach is schematically depicted in Figure 2b (see the Methods section for details). Figure 2c shows the scanning electron microscopy (SEM) images of a representative SiN waveguide before the chromium mask was removed to avoid charging.

After fabrication, the samples were characterized using our confocal microscope to address individual waveguide-coupled quantum emitters. Figure 3a shows a confocal PL intensity map of a waveguide segment. There are a few quantum emitters clearly resolved within this 10 μ m long segment, which is outlined by the dashed lines. The number of observed emitters is in-line with their density in the original SiN films. These quantum emitters can now be excited by coupling laser light into the waveguide via the grating couplers. Figure 3b is a wide-field image of the waveguide taken using a charged coupled camera (CCD) showing transmission of the 532 nm laser pump light with polarization orthogonal to the waveguide axis. The laser intensity at the outcoupling spot is clearly observed, indicating reasonable incoupling and outcoupling efficiencies of the grating couplers (see more data on laser coupling in the Supporting Information). The laser light coupled to the waveguide excites quantum emitters as it propagates. The PL from quantum emitters partially outcouples to the far field and can be observed using the CCD camera. Figure 3c shows the emission from spatially isolated quantum emitters positioned along the waveguide. Additional CCD images of the waveguides with quantum emitters are provided in the Supporting Information, confirming the

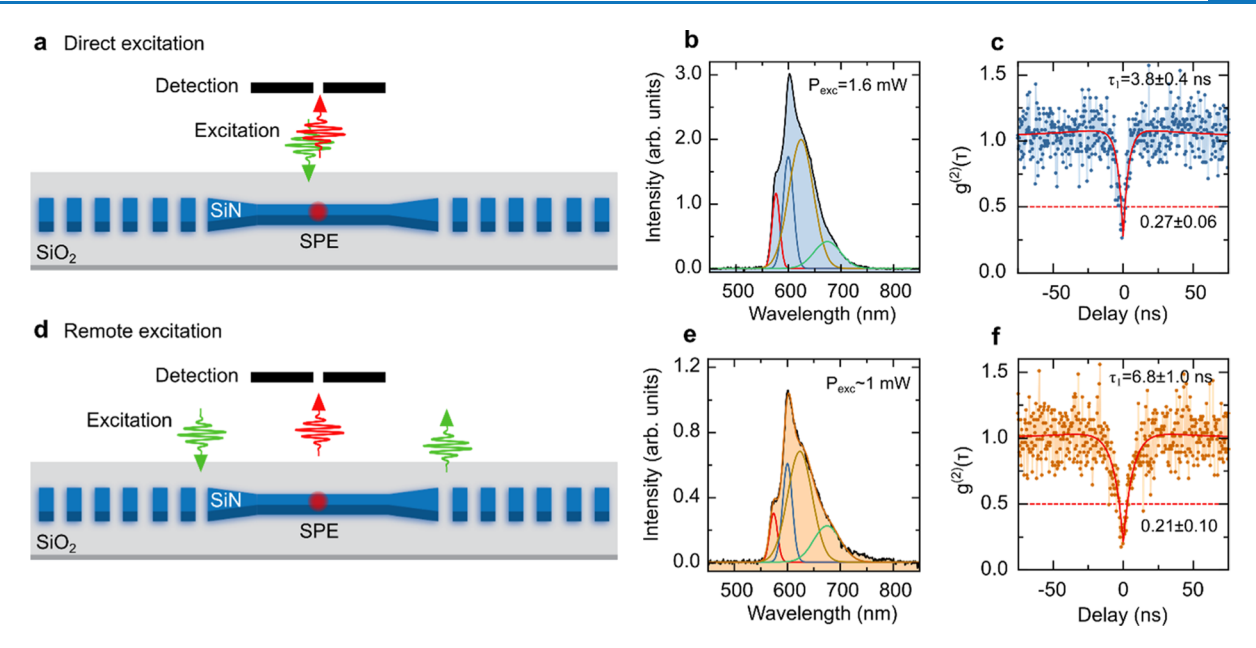


Figure 4. Photophysical properties of the selected quantum emitter measured in two configurations. (a) Direct excitation measurements of the quantum emitter showing its (b) PL spectrum and (c) second-order autocorrelation histogram $g^{(2)}(\tau)$. (d) Remote excitation measurements of the quantum emitter with the corresponding (e) PL spectrum and (f) second-order autocorrelation histogram $g^{(2)}(\tau)$. Both measurement schemes give comparable results.

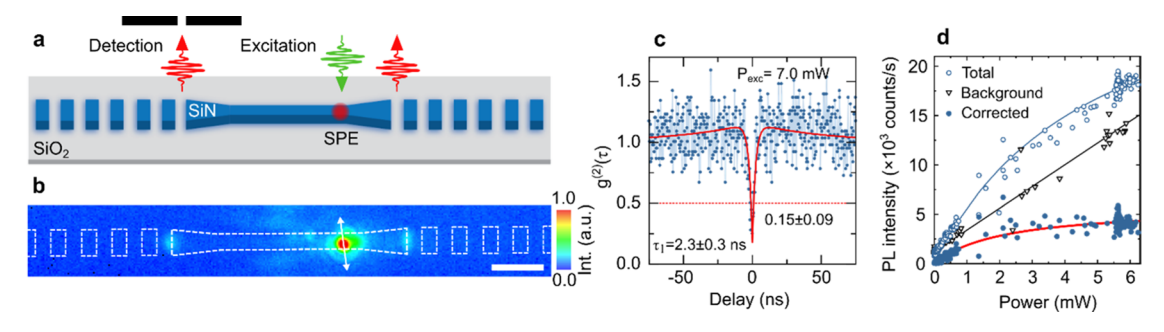


Figure 5. Observation of single-photon emission coupled to a waveguide mode. (a) Schematic of the decoupled excitation and detection scheme. (b) CCD image of the quantum emitter in the waveguide directly excited by the laser light. The white double ended arrow indicates the dipole orientation. The scale bar is 2 μ m. The excitation light is filtered out using a 550 nm long pass filter. Emission is collected from the left grating coupler: (c) Second-order autocorrelation histogram $g^{(2)}(\tau)$ fitted with the three-level model (red curve), yielding a $g^{(2)}(0)$ of 0.15 \pm 0.09, (d) PL saturation measurement for the given emitter, indicating a saturation power of $P_{\text{sat}} = 2.1 \pm 0.3$ mW and a maximum intensity of $I_{\infty} = 6 \times 10^3$ counts/s.

appearance of at least several quantum emitters per waveguide using our alignment-free approach. The same quantum emitter is circled in red in both the confocal PL map (Figure 3a) and the CCD image (Figure 3b) and was selected for further analysis.

Using the selected quantum emitter, we explored different excitation detection schemes for addressing individual emitters embedded in a SiN waveguide. First, we probed the emitter in a conventional confocal measurement scheme, where the PL signal is collected directly from the excitation spot (Figure 4a). The PL spectrum has a similar structure to those of SiN quantum emitters at room temperature reported previously, the structure of which is yet to be fully understood (Figure 4b).¹

The PL spectrum can be fitted with four Gaussian curves with peak wavelengths of 576, 600, 624, and 674 nm, which are within the spectral range typically observed for these emitters. The second-order autocorrelation $g^{(2)}(\tau)$ measurements reveal a clear dip below 0.5 at zero delay time, indicating that the selected emitter is likely a single-photon source. The

experimental data were fitted with a two-exponential model $g^{(2)}(\tau)=1-A\exp(|\tau|/\tau_1)+B\exp(|\tau|/\tau_1)$, where A,B,τ_1 , and τ_2 are the fitting parameters. The fitting parameter τ_1 describes the lifetime of transitions between the ground and excited states of a two-level system, while the parameter τ_2 gives the lifetime of a metastable state. Fitting the experimental data provides a $g^{(2)}(0)$ value at a zero delay time of 0.27 ± 0.06 —without background correction or spectral filtering. This suggests that the actual single-photon emission purity could be higher than that measured (Figure 4c). This $g^{(2)}(0)$ value is also within the expected range compared to previously reported results. The emission lifetime estimated from the $g^{(2)}(\tau)$ measurements was found to be $\tau_1=3.8\pm0.4$ ns, which is characteristic for this type of emitters.

Next, we used a scheme with the excitation and detection spots decoupled. For the selected emitter, we coupled the laser light to the waveguide through the grating coupler and collected the PL signal outcoupled to the far field directly from the emitter, as shown schematically in Figure 4d. The PL spectrum matches that measured using the direct excitation

scheme, confirming that we addressed the same quantum emitter in both measurements (Figure 4e).

The PL intensity is found to be lower than for the direct excitation scheme. This is explained by the lower excitation power reaching the emitter through the waveguide due to the coupling efficiency of the grating couplers. Fitting the second-order autocorrelation histogram shown in Figure 4f gives a $g^{(2)}(0)$ value comparable, within experimental uncertainty, to that measured using the direct excitation scheme. However, the emission lifetime is estimated to be $\tau_1 = 6.8 \pm 1.0$ ns, which may be a result the lower excitation power reaching the emitter. ¹⁸

Finally, we studied the coupling of single-photon emission from a quantum emitter to the waveguide mode. For the given waveguides, simultaneous remote excitation and waveguide detection will result in excitation of multiple emitters within the waveguide (Figure 3c), making the interpretation of the results unclear (Supporting Information, Figure S4). Therefore, we again used the decoupled excitation and detection scheme, but with the emitter excited directly and the emission coupled to a waveguide and collected remotely from one of the grating couplers, as shown in Figure 5a.

Direct excitation allows for a particular emitter of choice to be addressed while avoiding the excitation of other emitters present in the waveguide. This method has previously been successfully used in similar configurations. ^{28,46,60} We used laser polarization aligned along and perpendicular to the waveguide axis and found no evidence of background intensity dependence with laser polarization due to the possible laser light coupling to the waveguide.

Figure 5b shows the CCD image of the PL emission after the 550 nm long-pass filter is used to remove the residual 532 nm excitation light. The waveguide outline is shown with the dashed white lines. The excitation spot appears particularly bright due to the high-power laser used to excite the emitter and emission partially outcoupled into the far field. The emission outcoupled at the grating couplers is also clearly visible in the CCD image. The white double ended arrow indicates the dipole orientation deduced from the polarization measurements of the emission collected from the same emitter directly at the excitation spot (Supporting Information, Figure S5). The emitter was found to be tilted only about 8° off the transverse orientation relative to the waveguide longitudinal axis. The emitter also appears to be shifted from the center position relative to the waveguide width (Figure 5b). However, we assumed that the emitter is positioned in the center of the waveguide for the upper bound estimation of the coupling efficiency β . For the given position and orientation of the emitter within the waveguide, we obtained a coupling efficiency β of 21% from the simulation (Supporting Information, Figure S2).

To confirm the single-photon nature of the outcoupled emission, we performed second-order autocorrelation $g^{(2)}(\tau)$ measurements using photons collected at one of the grating couplers. The $g^{(2)}(\tau)$ histogram shown in Figure 5c was collected over the course of 30 min to obtain a sufficient signal-to-noise ratio. The $g^{(2)}(0)$ value at a zero delay time shows a pronounced dip below 0.5, indicating that the outcoupled light maintains single-photon emission statistics. The fitting of the experimental data was once again performed using the two-exponential model characteristic for three-level systems. The $g^{(2)}(\tau)$ value at zero delay time obtained from the fit was found to be $g^{(2)}(0) = 0.15 \pm 0.09$. This value agrees with the $g^{(2)}(0)$

values obtained from second-order autofluorescence histograms measured for the same emitter under direct collection of the emission at the excitation spot (Supporting Information, Figures S6, S7). Additional waveguides showing coupling of the single-photon emission into the waveguide mode are shown in the Supporting Information (Figure S8).

Finally, we evaluated the waveguide outcoupled emission rate and compared it with the coupling efficiency β obtained from simulation. This was carried out by first performing saturation measurements of the emission outcoupled out of the waveguide through the grating coupler (Figure 5d). The total emission rate was background corrected. The background was collected at a laser position without emitters, and counts were measured at different excitation powers. Then, the background counts were subtracted from the total emission counts. This background subtracted experimental data were then fitted with the equation $I(P) = I_{\infty} \times P/(P + P_{\text{sat}})$ with the fitting parameters I_{∞} and $P_{\rm sat}$ corresponding to the maximum count rate and saturation power, respectively. I_{∞} and P_{sat} were found to be 6×10^3 counts/s (cps) and 2.1 ± 0.3 mW, respectively. We repeated this analysis for the emission collected directly from the same emitter. The fitting of the background-corrected saturation curve yielded a maximum emission rate of $I_{\infty} = 412$ \times 10³ cps and a saturation power of $P_{\text{sat}} = 0.8 \pm 0.04 \text{ mW}$ (Supporting Information, Figure S7).

For the position and orientation of the emitter described above, the simulated coupling efficiency β is 21%. The outcoupling efficiency from the waveguide to the far field through the grating coupler is $\eta = 22\%$. From simulation, we also estimated that only about 10% of the total emission from the emitter is collected by the objective. Therefore, to extrapolate the total brightness of our emitter from the count rate measured via the objective, we multiplied it by 10. Thus, the extrapolated total brightness of our emitter is 4120 \times 10³ cps. Applying this estimate for the emitter brightness, we can estimate the count rate predicted by the simulation out of one grating coupler to be $0.5 \times \eta \times \beta \times 4120 \times 10^3 = 95 \times 10^3$ cps. This value is notably larger than the emission rate obtained experimentally $(6 \times 10^3 \text{ cps})$ (Figure 5d). The lower emission rate observed in the experiment may be due to a variety of factors including the displacement of the emitter from the center of the waveguide and fabrication imperfections such as roughness and size variations. The emission coupling to the fundamental waveguide mode can be substantially improved with topology-optimized couplers,61 while the collection efficiency can be increased by using fiber end-fire coupling, which can theoretically provide an up to 86% efficiency. 62

CONCLUSIONS

In this work, we demonstrated the first realization of low-autofluorescence SiN waveguides with intrinsic single-photon emitters that preserve their photophysical characteristics after fabrication. The SiN waveguides developed in this work utilize a technology-ready material platform and feature native quantum emitters, thus promising to enable the realization of scalable QPICs with a seamless integration of single-photon sources. Notably, the emitters discovered in SiN provide a practical alternative to the complex, multi-material integration schemes of single-photon emitters with the SiN platform previously reported. The proposed integrated quantum emitters in SiN have great potential to enable a low-loss and scalable quantum photonic platform that is mature in terms of

planar fabrication, quality control, and integration. Our findings call for further studies of SiN quantum emitters aimed at gaining a deeper understanding of their structure, control of their properties, and schemes for site-controlled fabrication.

METHODS

Sample Growth and Emitter Activation. The samples with SiN quantum emitters were prepared following the fabrication procedure developed in our previous work. The SiN films were grown using a high-density plasma chemical vapor deposition system (Plasma-Therm Apex SLR) on commercially available silicon substrates coated with 3 μm thick SiO₂ (Rogue Valley Microdevices), making them suitable for waveguide fabrication. We used nitrogen-rich growth conditions with a ratio of silicon to nitrogen precursors N₂/ SiH₄ of 1.74, resulting in non-stoichiometric SiN. As was found in our previous work, these growth conditions give SiN films with low background autofluorescence in the visible spectral range, similar to nitrogen-rich SiN reported in the literature.⁵⁸ Single-photon emitters were generated by post-growth RTA for 120 s at a temperature of 1100 °C in a nitrogen atmosphere using a Jipelec Jetfirst RTA system. The described procedure was found to provide reproducible fabrication of low autofluorescence SiN films with bright, stable, and linearly polarized quantum emitters operating at room temperature.

Waveguide Design and Fabrication. All waveguides and outcouplers were designed and simulated using a commercial Maxwell solver (Lumerical) using the 3D finite-difference time-domain (FDTD) method. The waveguide dimensions were found to be 250 nm tall by 600 nm wide such that it supports the fundamental waveguide mode at the given emission wavelength. These dimensions were found assuming a refractive index 1.7 and a central wavelength of 600 nm. The quantum emitter is modeled with an electric dipole polarized in the plane of the substrate perpendicular to the propagation axis. Since the dipole is not in a homogeneous medium, the simulated coupling efficiencies β were normalized with the corresponding Purcell factor. The outcoupled field was calculated from a flux through a horizontal plane placed 1 μ m above the grating outcoupler. Outcoupling efficiency η is defined as the ratio of the Poynting vector flux through this plane to the fundamental waveguide mode energy.

A large array of waveguides was fabricated on a single substrate to increase the probability of creating a waveguide with an emitter optimally oriented for efficient coupling. The waveguides were patterned into an electron beam resist (ZEP520A) via electron beam lithography. Following the development of the resist, a 20 nm chromium film was evaporated onto the sample and lifted off to form a hard mask. The silicon nitride layer was then etched by inductively coupled plasma reactive ion etching. The chromium hard mask was then chemically removed using chrome etching (KMG CR-16). The high density of quantum emitters in the original SiN ensured the integration of at least a few emitters in each waveguide without any special alignment procedures.

Photoluminescence Measurements. The optical characterization of SiN waveguide-integrated quantum emitters was performed at room temperature. We used a custom-made scanning confocal microscope based on a commercial inverted microscope body (Ti–U, Nikon). The microscope was equipped with a 100 μ m pinhole and a 100× air objective with a numerical aperture of 0.90 (Nikon). We estimate that

the laser pump spot size on the sample was around 1 μ m. The confocal scanning was performed with the objective mounted on a piezo stage (P-561, Physik Instrumente) driven by a controller (E-712, Physik Instrumente) and interfaced with LabVIEW (National Instruments). We used a 200 mW continuous wave 532 nm diode-pumped solid-state laser (Lambda beam PB 532-200 DPSS, RGB Photonics) for the optical excitation of emitters. The excitation light and PL signal were uncoupled using a 550 nm long-pass dichroic mirror (DMLP550, Thorlabs). The remaining pump power was further suppressed using a 550 nm long-pass filter (FEL0550, Thorlabs) installed in front of the detectors. We acquired the emission using an avalanche detector with 69% quantum efficiency at 650 nm (SPCM-AQRH, Excelitas) for singlephoton detection during scanning. To reveal the quantum nature of the emitters, second-order autocorrelation function $g^{(2)}(\tau)$ measurements were performed using a Hanbury, Brown, and Twiss (HBT) setup composed of two avalanche detectors with a 30 ps time resolution and a 35% quantum efficiency at 650 nm (PDM, Micro-Photon Devices) and an acquisition card with a 4 ps internal jitter (SPC-150, Becker & Hickl). For the excitation of an emitter through the waveguide, we walked the laser spot along the waveguide using two mirrors in front of the microscope. The detection spot was kept at a grating coupler or a region of interest along the waveguide.

ASSOCIATED CONTENT

Supporting Information

The Supporting Information is available free of charge at https://pubs.acs.org/doi/10.1021/acsphotonics.2c00750.

Simulation of coupling efficiency, polarization-dependent laser coupling to a waveguide, additional CCD images of single-photon emitters integrated in SiN waveguides, polarization measurements, power-dependent second-order autocorrelation histograms, comparison of direct and waveguide outcoupled single-photon emissions, and additional measurements of single-photon emission coupled to waveguides (PDF)

AUTHOR INFORMATION

Corresponding Authors

Alexander Senichev — Elmore Family School of Electrical and Computer Engineering, Birck Nanotechnology Center and Purdue Quantum Science and Engineering Institute, Purdue University, West Lafayette, Indiana 47907, United States; Quantum Science Center, Department of Energy, A National Quantum Information Science Research Center of the U.S., Oak Ridge, Tennessee 37931, United States; orcid.org/0000-0003-2789-123X; Email: senichev@purdue.edu

Vladimir M. Shalaev — Elmore Family School of Electrical and Computer Engineering, Birck Nanotechnology Center and Purdue Quantum Science and Engineering Institute, Purdue University, West Lafayette, Indiana 47907, United States; Quantum Science Center, Department of Energy, A National Quantum Information Science Research Center of the U.S., Oak Ridge, Tennessee 37931, United States; Email: shalaev@purdue.edu

Authors

Samuel Peana – Elmore Family School of Electrical and Computer Engineering, Birck Nanotechnology Center and

- Purdue Quantum Science and Engineering Institute, Purdue University, West Lafayette, Indiana 47907, United States; Quantum Science Center, Department of Energy, A National Quantum Information Science Research Center of the U.S., Oak Ridge, Tennessee 37931, United States
- Zachariah O. Martin Elmore Family School of Electrical and Computer Engineering, Birck Nanotechnology Center and Purdue Quantum Science and Engineering Institute, Purdue University, West Lafayette, Indiana 47907, United States; Quantum Science Center, Department of Energy, A National Quantum Information Science Research Center of the U.S., Oak Ridge, Tennessee 37931, United States
- Omer Yesilyurt Elmore Family School of Electrical and Computer Engineering, Birck Nanotechnology Center and Purdue Quantum Science and Engineering Institute, Purdue University, West Lafayette, Indiana 47907, United States; Quantum Science Center, Department of Energy, A National Quantum Information Science Research Center of the U.S., Oak Ridge, Tennessee 37931, United States; orcid.org/0000-0002-9829-5219
- Demid Sychev Elmore Family School of Electrical and Computer Engineering, Birck Nanotechnology Center and Purdue Quantum Science and Engineering Institute, Purdue University, West Lafayette, Indiana 47907, United States; Quantum Science Center, Department of Energy, A National Quantum Information Science Research Center of the U.S., Oak Ridge, Tennessee 37931, United States
- Alexei S. Lagutchev Elmore Family School of Electrical and Computer Engineering, Birck Nanotechnology Center and Purdue Quantum Science and Engineering Institute, Purdue University, West Lafayette, Indiana 47907, United States; Quantum Science Center, Department of Energy, A National Quantum Information Science Research Center of the U.S., Oak Ridge, Tennessee 37931, United States
- Alexandra Boltasseva Elmore Family School of Electrical and Computer Engineering, Birck Nanotechnology Center and Purdue Quantum Science and Engineering Institute, Purdue University, West Lafayette, Indiana 47907, United States; Quantum Science Center, Department of Energy, A National Quantum Information Science Research Center of the U.S., Oak Ridge, Tennessee 37931, United States;

 orcid.org/0000-0001-8905-2605

Complete contact information is available at: https://pubs.acs.org/10.1021/acsphotonics.2c00750

Author Contributions

The manuscript was written through contributions of all authors. All authors have given approval to the final version of the manuscript. The authors thank Vahagn Mkhitaryan for useful discussions.

Funding

This work was supported by the U.S. Department of Energy (DOE), Office of Science through the Quantum Science Center (QSC), a National Quantum Information Science Research Center, National Science Foundation (NSF) grant 2015025-ECCS, and Purdue's Elmore ECE Emerging Frontiers Center "The Crossroads of Quantum and AI."

Notes

The authors declare no competing financial interest.

REFERENCES

- (1) Senichev, A.; Martin, Z. O.; Peana, S.; Sychev, D.; Xu, X.; Lagutchev, A. S.; Boltasseva, A.; Shalaev, V. M. Room-Temperature Single-Photon Emitters in Silicon Nitride. *Sci. Adv.* **2021**, *7*, No. eabj062.
- (2) Aharonovich, I.; Englund, D.; Toth, M. Solid-State Single-Photon Emitters. *Nat. Photonics* **2016**, *10*, 631–641.
- (3) Azuma, K.; Tamaki, K.; Lo, H.-K. All-Photonic Quantum Repeaters. *Nat. Commun.* **2015**, *6*, 6787.
- (4) Borregaard, J.; Pichler, H.; Schröder, T.; Lukin, M. D.; Lodahl, P.; Sørensen, A. S. One-Way Quantum Repeater Based on Near-Deterministic Photon-Emitter Interfaces. *Phys. Rev. X* **2020**, *10*, 21071.
- (5) Bhaskar, M. K.; Riedinger, R.; Machielse, B.; Levonian, D. S.; Nguyen, C. T.; Knall, E. N.; Park, H.; Englund, D.; Lončar, M.; Sukachev, D. D.; Lukin, M. D. Experimental Demonstration of Memory-Enhanced Quantum Communication. *Nature* **2020**, *580*, 60–64.
- (6) Maletinsky, P.; Hong, S.; Grinolds, M. S.; Hausmann, B.; Lukin, M. D.; Walsworth, R. L.; Loncar, M.; Yacoby, A. A Robust Scanning Diamond Sensor for Nanoscale Imaging with Single Nitrogen-Vacancy Centres. *Nat. Nanotechnol.* **2012**, *7*, 320–324.
- (7) Uppu, R.; Midolo, L.; Zhou, X.; Carolan, J.; Lodahl, P. Quantum-Dot-Based Deterministic Photon-Emitter Interfaces for Scalable Photonic Quantum Technology. *Nat. Nanotechnol.* **2021**, *16*, 1308–1317.
- (8) Moody, G.; Sorger, V. J.; Blumenthal, D. J.; Juodawlkis, P. W.; Loh, W.; Sorace-Agaskar, C.; Jones, A. E.; Balram, K. C.; Matthews, J. C. F.; Laing, A.; Davanco, M.; Chang, L.; Bowers, J. E.; Quack, N.; Galland, C.; Aharonovich, I.; Wolff, M. A.; Schuck, C.; Sinclair, N.; Lončar, M.; Komljenovic, T.; Weld, D.; Mookherjea, S.; Buckley, S.; Radulaski, M.; Reitzenstein, S.; Pingault, B.; Machielse, B.; Mukhopadhyay, D.; Akimov, A.; Zheltikov, A.; Agarwal, G. S.; Srinivasan, K.; Lu, J.; Tang, H. X.; Jiang, W.; McKenna, T. P.; Safavi-Naeini, A. H.; Steinhauer, S.; Elshaari, A. W.; Zwiller, V.; Davids, P. S.; Martinez, N.; Gehl, M.; Chiaverini, J.; Mehta, K. K.; Romero, J.; Lingaraju, N. B.; Weiner, A. M.; Peace, D.; Cernansky, R.; Lobino, M.; Diamanti, E.; Vidarte, L. T.; Camacho, R. M. Roadmap on Integrated Quantum Photonics. J. Phys. Photonics 2022, 4, 012501.
- (9) Bogdanov, S.; Shalaginov, M. Y.; Boltasseva, A.; Shalaev, V. M. Material Platforms for Integrated Quantum Photonics. *Opt. Mater. Express* **2017**, *7*, 111.
- (10) Lee, J.; Leong, V.; Kalashnikov, D.; Dai, J.; Gandhi, A.; Krivitsky, L. A. Integrated Single Photon Emitters. *AVS Quantum Sci* **2020**, *2*, 031701.
- (11) Lodahl, P. Quantum-Dot Based Photonic Quantum Networks. *Quantum Sci. Technol.* **2018**, *3*, 013001.
- (12) Uppu, R.; Pedersen, F. T.; Ying, W.; Olesen, C. T.; Papon, C.; Zhou, X.; Midolo, L.; Scholz, S.; Wieck, A. D.; Ludwig, A.; Lodahl, P. Scalable Integrated Single-Photon Source. *Sci. Adv.* **2020**, *6*, No. eabc8268.
- (13) Aharonovich, I.; Castelletto, S.; Simpson, D. A.; Su, C.-H.; Greentree, A. D.; Prawer, S. Diamond-Based Single-Photon Emitters. *Reports Prog. Phys.* **2011**, *74*, 076501.
- (14) Schröder, T.; Mouradian, S. L.; Zheng, J.; Trusheim, M. E.; Walsh, M.; Chen, E. H.; Li, L.; Bayn, I.; Englund, D. Quantum Nanophotonics in Diamond [Invited]. *J. Opt. Soc. Am. B* **2016**, 33, B65.
- (15) Bradac, C.; Gao, W.; Forneris, J.; Trusheim, M. E.; Aharonovich, I. Quantum Nanophotonics with Group IV Defects in Diamond. *Nat. Commun.* **2019**, *10*, 5625.
- (16) Lohrmann, A.; Johnson, B. C.; McCallum, J. C.; Castelletto, S. A Review on Single Photon Sources in Silicon Carbide. *Reports Prog. Phys.* **2017**, *80*, 034502.
- (17) Son, N. T.; Anderson, C. P.; Bourassa, A.; Miao, K. C.; Babin, C.; Widmann, M.; Niethammer, M.; Ul Hassan, J.; Morioka, N.; Ivanov, I. G.; Kaiser, F.; Wrachtrup, J.; Awschalom, D. D. Developing Silicon Carbide for Quantum Spintronics. *Appl. Phys. Lett.* **2020**, *116*, 190501.

- (18) Lienhard, B.; Schröder, T.; Mouradian, S.; Dolde, F.; Tran, T. T.; Aharonovich, I.; Englund, D. Bright and Photostable Single-Photon Emitter in Silicon Carbide. *Optica* **2016**, *3*, 768.
- (19) Lukin, D. M.; Guidry, M. A.; Vučković, J. Integrated Quantum Photonics with Silicon Carbide: Challenges and Prospects. *PRX Quantum* **2020**, *1*, 020102.
- (20) Tran, T. T.; Elbadawi, C.; Totonjian, D.; Lobo, C. J.; Grosso, G.; Moon, H.; Englund, D. R.; Ford, M. J.; Aharonovich, I.; Toth, M. Robust Multicolor Single Photon Emission from Point Defects in Hexagonal Boron Nitride. *ACS Nano* **2016**, *10*, 7331–7338.
- (21) Kubanek, A. Coherent Quantum Emitters in Hexagonal Boron Nitride. *Adv. Quantum Technol.* **2022**, *3*, 2200009.
- (22) Gottscholl, A.; Kianinia, M.; Soltamov, V.; Orlinskii, S.; Mamin, G.; Bradac, C.; Kasper, C.; Krambrock, K.; Sperlich, A.; Toth, M.; Aharonovich, I.; Dyakonov, V. Initialization and Read-out of Intrinsic Spin Defects in a van Der Waals Crystal at Room Temperature. *Nat. Mater.* **2020**, *19*, 540–545.
- (23) Hausmann, B. J. M.; Shields, B.; Quan, Q.; Maletinsky, P.; McCutcheon, M.; Choy, J. T.; Babinec, T. M.; Kubanek, A.; Yacoby, A.; Lukin, M. D.; Lončar, M. Integrated Diamond Networks for Quantum Nanophotonics. *Nano Lett* **2012**, *12*, 1578–1582.
- (24) Zhang, J. L.; Sun, S.; Burek, M. J.; Dory, C.; Tzeng, Y.-K.; Fischer, K. A.; Kelaita, Y.; Lagoudakis, K. G.; Radulaski, M.; Shen, Z.-X.; Melosh, N. A.; Chu, S.; Lončar, M.; Vučković, J. Strongly Cavity-Enhanced Spontaneous Emission from Silicon-Vacancy Centers in Diamond. *Nano Lett* **2018**, *18*, 1360–1365.
- (25) Nguyen, C. T.; Sukachev, D. D.; Bhaskar, M. K.; Machielse, B.; Levonian, D. S.; Knall, E. N.; Stroganov, P.; Riedinger, R.; Park, H.; Lončar, M.; Lukin, M. D. Quantum Network Nodes Based on Diamond Qubits with an Efficient Nanophotonic Interface. *Phys. Rev. Lett.* **2019**, *123*, 183602.
- (26) Lukin, D. M.; Dory, C.; Guidry, M. A.; Yang, K. Y.; Mishra, S. D.; Trivedi, R.; Radulaski, M.; Sun, S.; Vercruysse, D.; Ahn, G. H.; Vučković, J. 4H-Silicon-Carbide-on-Insulator for Integrated Quantum and Nonlinear Photonics. *Nat. Photonics* **2020**, *14*, 330–334.
- (27) Fröch, J. E.; Spencer, L. P.; Kianinia, M.; Totonjian, D. D.; Nguyen, M.; Gottscholl, A.; Dyakonov, V.; Toth, M.; Kim, S.; Aharonovich, I. Coupling Spin Defects in Hexagonal Boron Nitride to Monolithic Bullseye Cavities. *Nano Lett* **2021**, *21*, 6549–6555.
- (28) Li, C.; Fröch, J. E.; Nonahal, M.; Tran, T. N.; Toth, M.; Kim, S.; Aharonovich, I. Integration of HBN Quantum Emitters in Monolithically Fabricated Waveguides. *ACS Photonics* **2021**, 8, 2966–2972.
- (29) Elshaari, A. W.; Pernice, W.; Srinivasan, K.; Benson, O.; Zwiller, V. Hybrid Integrated Quantum Photonic Circuits. *Nat. Photonics* **2020**, *14*, 285–298.
- (30) Kim, J.; Aghaeimeibodi, S.; Carolan, J.; Englund, D.; Waks, E. Hybrid Integration Methods for On-Chip Quantum Photonics. *Optica* **2020**, *7*, 291–308.
- (31) Wan, N. H.; Lu, T.-J.; Chen, K. C.; Walsh, M. P.; Trusheim, M. E.; De Santis, L.; Bersin, E. A.; Harris, I. B.; Mouradian, S. L.; Christen, I. R.; Bielejec, E. S.; Englund, D. Large-Scale Integration of Artificial Atoms in Hybrid Photonic Circuits. *Nature* **2020**, *583*, 226–231.
- (32) Aghaeimeibodi, S.; Desiatov, B.; Kim, J.-H.; Lee, C.-M.; Buyukkaya, M. A.; Karasahin, A.; Richardson, C. J. K.; Leavitt, R. P.; Lončar, M.; Waks, E. Integration of Quantum Dots with Lithium Niobate Photonics. *Appl. Phys. Lett.* **2018**, *113*, 221102.
- (33) Davanco, M.; Liu, J.; Sapienza, L.; Zhang, C. Z.; De Miranda Cardoso, J. V.; Verma, V.; Mirin, R.; Nam, S. W.; Liu, L.; Srinivasan, K. Heterogeneous Integration for On-Chip Quantum Photonic Circuits with Single Quantum Dot Devices. *Nat. Commun.* **2017**, *8*, 889
- (34) Mnaymneh, K.; Dalacu, D.; McKee, J.; Lapointe, J.; Haffouz, S.; Weber, J. F.; Northeast, D. B.; Poole, P. J.; Aers, G. C.; Williams, R. L. On-Chip Integration of Single Photon Sources via Evanescent Coupling of Tapered Nanowires to SiN Waveguides. *Adv. Quantum Technol.* **2020**, *3*, 1900021.

- (35) Zadeh, I. E.; Elshaari, A. W.; Jöns, K. D.; Fognini, A.; Dalacu, D.; Poole, P. J.; Reimer, M. E.; Zwiller, V. Deterministic Integration of Single Photon Sources in Silicon Based Photonic Circuits. *Nano Lett* **2016**, *16*, 2289–2294.
- (36) Katsumi, R.; Ota, Y.; Osada, A.; Yamaguchi, T.; Tajiri, T.; Kakuda, M.; Iwamoto, S.; Akiyama, H.; Arakawa, Y. Quantum-Dot Single-Photon Source on a CMOS Silicon Photonic Chip Integrated Using Transfer Printing. *APL Photonics* **2019**, *4*, 036105.
- (37) Fryett, T. K.; Chen, Y.; Whitehead, J.; Peycke, Z. M.; Xu, X.; Majumdar, A. Encapsulated Silicon Nitride Nanobeam Cavity for Hybrid Nanophotonics. *ACS Photonics* **2018**, *5*, 2176–2181.
- (38) Fröch, J. E.; Kim, S.; Mendelson, N.; Kianinia, M.; Toth, M.; Aharonovich, I. Coupling Hexagonal Boron Nitride Quantum Emitters to Photonic Crystal Cavities. *ACS Nano* **2020**, *14*, 7085–7091
- (39) Elshaari, A. W.; Skalli, A.; Gyger, S.; Nurizzo, M.; Schweickert, L.; Esmaeil Zadeh, I.; Svedendahl, M.; Steinhauer, S.; Zwiller, V. Deterministic Integration of HBN Emitter in Silicon Nitride Photonic Waveguide. *Adv. Quantum Technol.* **2021**, *4*, 2100032.
- (40) Fehler, K. G.; Ovvyan, A. P.; Gruhler, N.; Pernice, W. H. P. P.; Kubanek, A. Efficient Coupling of an Ensemble of Nitrogen Vacancy Center to the Mode of a High-Q, Si3N4 Photonic Crystal Cavity. *ACS Nano* **2019**, *13*, 6891–6898.
- (41) Fehler, K. G.; Ovvyan, A. P.; Antoniuk, L.; Lettner, N.; Gruhler, N.; Davydov, V. A.; Agafonov, V. N.; Pernice, W. H. P.; Kubanek, A. Purcell-Enhanced Emission from Individual SiV Center in Nanodiamonds Coupled to a Si₃N₄-Based, Photonic Crystal Cavity. *Nanophotonics* **2020**, *9*, 3655–3662.
- (42) Berhane, A. M.; Jeong, K.; Bodrog, Z.; Fiedler, S.; Schröder, T.; Triviño, N. V.; Palacios, T.; Gali, A.; Toth, M.; Englund, D.; Aharonovich, I. Bright Room-Temperature Single-Photon Emission from Defects in Gallium Nitride. *Adv. Mater.* **2017**, *29*, 1605092.
- (43) Zhou, Y.; Wang, Z.; Rasmita, A.; Kim, S.; Berhane, A.; Bodrog, Z.; Adamo, G.; Gali, A.; Aharonovich, I.; Gao, W.-B. Room Temperature Solid-State Quantum Emitters in the Telecom Range. *Sci. Adv.* 2018, 4, No. eaar3580.
- (44) Bishop, S. G.; Hadden, J. P.; Alzahrani, F.; Hekmati, R.; Huffaker, D. L.; Langbein, W. W.; Bennett, A. J. Room Temperature Quantum Emitter in Aluminum Nitride. *ACS Photonics* **2020**, *7*, 1636–1641.
- (45) Xue, Y.; Wang, H.; Xie, N.; Yang, Q.; Xu, F.; Shen, B.; Shi, J.; Jiang, D.; Dou, X.; Yu, T.; Sun, B. Single-Photon Emission from Point Defects in Aluminum Nitride Films. *J. Phys. Chem. Lett.* **2020**, *11*, 2689–2694.
- (46) Lu, T.-J.; Lienhard, B.; Jeong, K.-Y.; Moon, H.; Iranmanesh, A.; Grosso, G.; Englund, D. Bright High-Purity Quantum Emitters in Aluminum Nitride Integrated Photonics. *ACS Photonics* **2020**, *7*, 2650–2657.
- (47) Xue, Y.; Wei, T.; Chang, H.; Liang, D.; Dou, X.; Sun, B. Experimental Optical Properties of Single-Photon Emitters in Aluminum Nitride Films. *J. Phys. Chem. C* **2021**, *125*, 11043–11047.
- (48) Redjem, W.; Durand, A.; Herzig, T.; Benali, A.; Pezzagna, S.; Meijer, J.; Kuznetsov, A. Y.; Nguyen, H. S.; Cueff, S.; Gérard, J.-M.; Robert-Philip, I.; Gil, B.; Caliste, D.; Pochet, P.; Abbarchi, M.; Jacques, V.; Dréau, A.; Cassabois, G. Single Artificial Atoms in Silicon Emitting at Telecom Wavelengths. *Nat. Electron.* **2020**, *3*, 738–743.
- (49) Hollenbach, M.; Berencén, Y.; Kentsch, U.; Helm, M.; Astakhov, G. V. Engineering Telecom Single-Photon Emitters in Silicon for Scalable Quantum Photonics. *Opt. Express* **2020**, *28*, 26111.
- (50) Prabhu, M.; Errando-Herranz, C.; De Santis, L.; Christen, I.; Chen, C.; Englund, D. R. Individually Addressable Artificial Atoms in Silicon Photonics. *Quantum Physics*, 2022; Vol. 4, 2202, 02342. arXiv ver. 1. https://arxiv.org/abs/2202.02342 (accessed 2022 31 08).
- (51) Ikeda, K.; Saperstein, R. E.; Alic, N.; Fainman, Y. Thermal and Kerr Nonlinear Properties of Plasma-Deposited Silicon Nitride/Silicon Dioxide Waveguides. *Opt. Express* **2008**, *16*, 12987.

- (52) Moss, D. J.; Morandotti, R.; Gaeta, A. L.; Lipson, M. New CMOS-Compatible Platforms Based on Silicon Nitride and Hydex for Nonlinear Optics. *Nat. Photonics* **2013**, *7*, 597–607.
- (53) Gaeta, A. L.; Lipson, M.; Kippenberg, T. Photonic-chip-based frequency combs. *Nat. Photonics* **2019**, *13*, 158–169.
- (\$4) Taballione, C.; Wolterink, T. A. W.; Lugani, J.; Eckstein, A.; Bell, B. A.; Grootjans, R.; Visscher, I.; Renema, J. J.; Geskus, D.; Roeloffzen, C. G. H.; Walmsley, I. A.; Pinkse, P. W. H.; Boller, K.-J.. 8×8 Programmable Quantum Photonic Processor Based on Silicon Nitride Waveguides. Frontiers in Optics/Laser Science; OSA: Washington, D.C., 2018; Vol. F114-JTu3A.58.
- (55) Dong, M.; Clark, G.; Leenheer, A. J.; Zimmermann, M.; Dominguez, D.; Menssen, A. J.; Heim, D.; Gilbert, G.; Englund, D.; Eichenfield, M. High-Speed Programmable Photonic Circuits in a Cryogenically Compatible, Visible—near-Infrared 200 Mm CMOS Architecture. *Nat. Photonics* **2022**, *16*, 59–65.
- (56) Arrazola, J. M.; Bergholm, V.; Brádler, K.; Bromley, T. R.; Collins, M. J.; Dhand, I.; Fumagalli, A.; Gerrits, T.; Goussev, A.; Helt, L. G.; Hundal, J.; Isacsson, T.; Israel, R. B.; Izaac, J.; Jahangiri, S.; Janik, R.; Killoran, N.; Kumar, S. P.; Lavoie, J.; Lita, A. E.; Mahler, D. H.; Menotti, M.; Morrison, B.; Nam, S. W.; Neuhaus, L.; Qi, H. Y.; Quesada, N.; Repingon, A.; Sabapathy, K. K.; Schuld, M.; Su, D.; Swinarton, J.; Száva, A.; Tan, K.; Tan, P.; Vaidya, V. D.; Vernon, Z.; Zabaneh, Z.; Zhang, Y. Quantum Circuits with Many Photons on a Programmable Nanophotonic Chip. *Nature* 2021, 591, 54–60.
- (57) Taballione, C.; Anguita, M. C.; de Goede, M.; Venderbosch, P.; Kassenberg, B.; Snijders, H.; Kannan, N.; Smith, D.; Epping, J. P.; van der Meer, R.; Pinkse, P. W. H.; van den Vlekkert, H.; Renema, J. J. 20-Mode Universal Quantum Photonic Processor arXiv (Quantum Physics). 2022; Vol. 17, 2203.01801, ver. 3. https://arxiv.org/abs/2203.01801 (accessed 2022 08 31). June
- (58) Smith, J.; Monroy-Ruz, J.; Rarity, J. G.; Balram, K. C. Single Photon Emission and Single Spin Coherence of a Nitrogen Vacancy Center Encapsulated in Silicon Nitride. *Appl. Phys. Lett.* **2020**, *116*, 134001.
- (59) Kim, D. S.; Yoon, S. G.; Jang, G. E.; Suh, S. J.; Kim, H.; Yoon, D. H. Refractive Index Properties of SiN Thin Films and Fabrication of SiN Optical Waveguide. *J. Electroceramics* **2006**, *17*, 315–318.
- (60) Errando-Herranz, C.; Schöll, E.; Picard, R.; Laini, M.; Gyger, S.; Elshaari, A. W.; Branny, A.; Wennberg, U.; Barbat, S.; Renaud, T.; Sartison, M.; Brotons-Gisbert, M.; Bonato, C.; Gerardot, B. D.; Zwiller, V.; Jöns, K. D. Resonance Fluorescence from Waveguide-Coupled, Strain-Localized, Two-Dimensional Quantum Emitters. *ACS Photonics* **2021**, *8*, 1069–1076.
- (61) Yesilyurt, O.; Kudyshev, Z. A.; Boltasseva, A.; Shalaev, V. M.; Kildishev, A. V. Efficient Topology-Optimized Couplers for On-Chip Single-Photon Sources. *ACS Photonics* **2021**, *8*, 3061–3068.
- (62) Cohen, J. D.; Meenehan, S. M.; Painter, O. Optical Coupling to Nanoscale Optomechanical Cavities for near Quantum-Limited Motion Transduction. *Opt. Express* **2013**, *21*, 11227.